OPTICS

Miniaturized spectrometers with a tunable van der Waals junction

Hoon Hahn Yoon[1,2]*, Henry A. Fernandez[1,2], Fedor Nigmatulin[1,2], Weiwei Cai[3], Zongyin Yang[4], Hanxiao Cui[5], Faisal Ahmed[1], Xiaoqi Cui[1,2], Md Gius Uddin[1,2], Ethan D. Minot[6], Harri Lipsanen[1], Kwanpyo Kim[7], Pertti Hakonen[2], Tawfique Hasan[8], Zhipei Sun[1,2]*

Miniaturized computational spectrometers, which can obtain incident spectra using a combination of device spectral responses and reconstruction algorithms, are essential for on-chip and implantable applications. Highly sensitive spectral measurement using a single detector allows the footprints of such spectrometers to be scaled down while achieving spectral resolution approaching that of benchtop systems. We report a high-performance computational spectrometer based on a single van der Waals junction with an electrically tunable transport-mediated spectral response. We achieve high peak wavelength accuracy (~0.36 nanometers), high spectral resolution (~3 nanometers), broad operation bandwidth (from ~405 to 845 nanometers), and proof-of-concept spectral imaging. Our approach provides a route toward ultraminiaturization and offers unprecedented performance in accuracy, resolution, and operation bandwidth for single-detector computational spectrometers.

Spectrometers are indispensable for various applications, including industrial inspection, chemical and biological characterization, and image sensing and analysis (1, 2). Their miniaturization with high spectral resolution and wide operation bandwidth is highly desirable to meet the emerging and future demands in portable and on-chip applications (1). However, conventional spectroscopy systems typically rely on bulky dispersive optical components (e.g., gratings) and detector or filter arrays, which impose strict restrictions on ultraminiaturization (2).

Common spectrometer miniaturization approaches therefore replace the functions of these dispersive optical elements through various schemes (fig. S1), including photonic crystals (3), metasurfaces (4), and compact interferometers (5). Recently, a profound technological leap has seen the emergence of miniaturized computational spectrometers, which leverage the power of mathematical algorithms for spectrum reconstruction (1). Examples of such approaches include quantum dot filter arrays on top of charge-coupled device sensors (6), bandgap engineered multiple nanowires (7), a single nanowire with bandgap gradation (8), Stark effect in black
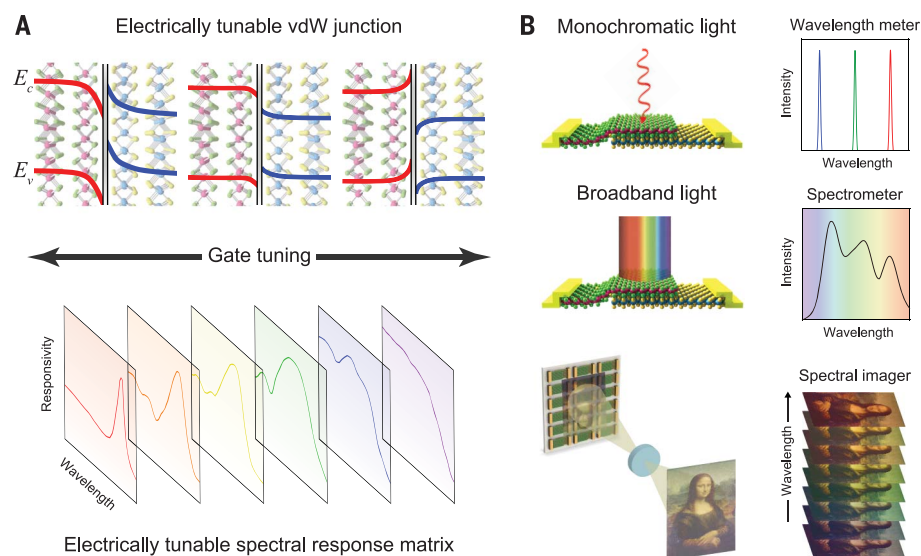
phosphorus (9), in situ perovskite modulation (10), and a single superconducting nanowire with tunable quantum efficiency (11). However, the performance and usability of these computational spectrometers remain limited: Spectral resolution and operation bandwidth are typically restricted by the number of integrated detectors (6–8), bandgap modulation limits (9, 10), and cryogenic operational requirements (11).

Photodetection with two-dimensional (2D) layered materials is advantageous owing to their strong light–matter interaction, atomically sharp interface, and electrically tunable

photoresponse (12–14). However, insufficient band structure modulation makes it challenging to achieve high-resolution broadband spectral sensing using a single 2D material. On the other hand, 2D material–based van der Waals (vdW) junctions offer highly tunable functionalities beyond the constituent materials (15–17) and could overcome these limitations. Specifically, we suggest that wavelength-dependent photodetection with vdW junctions recently exploited for optoelectronic logic computing (18, 19) and color sensing (20, 21) could also be key to high-resolution computational spectral sensing.

Here, we demonstrate a high-performance ultraminiaturized computational spectrometer using a single vdW junction with an electrically tunable transport-mediated spectral response. Our device, with its footprint defined by the junction size (~22 μm by 8 μm) shows unprecedented performance for a single-detector computational spectrometer, with the ability to resolve peak monochromatic wavelengths with ~0.36 nm accuracy, reconstruct broadband spectra with ~3 nm resolution, and acquire spectral images by spectral scanning. Our single-junction spectrometer concept can be extended to other tunable junctions to achieve high spectral resolution and broad operation bandwidth with its ultracompact size, representing the ultimate miniaturization strategy without sacrificing spectrometer performance.

The performance of computational spectrometers relies on the variability of their wavelength-dependent photoresponsivity (1, 6–11). The single-detector miniaturized spectrometers reported thus far are limited by

[1]Department of Electronics and Nanoengineering, Aalto University, Espoo 02150, Finland. [2]QTF Centre of Excellence, Department of Applied Physics, Aalto University, Aalto 00076, Finland. [3]Key Lab of Education Ministry for Power Machinery and Engineering, School of Mechanical Engineering, Shanghai Jiao Tong University, Shanghai 200240, China. [4]College of Information Science and Electronic Engineering and State Key Laboratory of Modern Optical Instrumentation, Zhejiang University, Hangzhou 310027, China. [5]School of Aeronautics and Astronautics, Sichuan University, Chengdu 610065, China. [6]Department of Physics, Oregon State University, Corvallis, OR 97331, USA. [7]Department of Physics, Yonsei University, Seoul 03722, Republic of Korea. [8]Cambridge Graphene Centre, University of Cambridge, Cambridge CB3 0FA, UK.
*Corresponding author. Email: hoonhahn.yoon@aalto.fi (H.H.Y.); zhipei.sun@aalto.fi (Z.S.)

Fig. 1. Ultraminiaturized spectrometer concept with a single vdW junction. (**A**) A typical gate-tunable band alignment at the vdW junction interface (top) with its distinct gate-tunable spectral response matrix (bottom). E_c (E_v) represents the conduction (valence) band edge. (**B**) Schematic of various application examples using a single-junction spectrometer: wavelength meter to distinguish peak wavelengths of monochromatic light (top), spectrometer to resolve broadband spectra (middle), and spectral imager to analyze spectral information of images (bottom).

their performance (9, 10) and usability (9, 11) owing to the limited band structure modulation and, consequently, the spectral response. In contrast, electrical tuning of the interfacial band alignment of a vdW junction (Fig. 1A, top panel) enables controllable and distinctive interlayer transport (15–17). Such electrically controllable interlayer transport allows for a tunable spectral response (Fig. 1A, bottom panel) with high sensitivity and variability over a wide spectral range (12–14), suggesting that a single vdW junction spectrometer could achieve substantially higher performance than previously reported spectrometers (supplementary text section ST1 and table S1). We combine an electrically tunable single vdW junction with a computational reconstruction algorithm for various applications (Fig. 1B). To experimentally realize our spectrometer concept, the following three steps are required (fig. S2): (i) measuring the gate-tunable spectral responses with multiple known incident spectra (i.e., the learning process), (ii) measuring the gate-tunable photocurrent of the unknown incident light to be analyzed (i.e., the testing process), and (iii) computing the spectral information of the unknown incident light on the basis of the results obtained in the learning and testing processes using the reconstruction algorithm (i.e., the reconstructing process).

The distinct and varied photoresponse of a vdW junction, tuned at different gate voltages and incident light wavelengths, is critical to our spectrometer (1). We choose a MoS_2/WSe_2 heterojunction (Fig. 2A) as an example, because of its distinct spectral response due to the gate-tunable photovoltaic effect from the visible to the near-infrared (22–28). The MoS_2/WSe_2 heterojunction is encapsulated by top and bottom hexagonal boron nitride (h-BN) layers for insulation and passivation, respectively (materials and methods section MM1). A monolayer graphene film below the stack is used as a local gate electrode for effective gate tuning. Each stacking layer was characterized by Raman spectroscopy and atomic force microscopy (fig. S3) to confirm the quality of the vdW heterostructure.

The transfer curves (drain-source current, I_{DS}, as a function of the gate-source voltage, V_{GS}) of the MoS_2 or WSe_2 channels and their heterojunction are measured at drain-source voltage $V_{DS} = 3$ V in dark conditions (Fig. 2B). The individual MoS_2 (WSe_2) channel exhibits n-type (p-type) characteristics owing to the donor (acceptor) impurities in MoS_2 (WSe_2). Thus, a depletion region and built-in electric field are expected at their vdW interface (22–28). The MoS_2/WSe_2 heterojunction is characterized by positive V_{DS} applied to the WSe_2 side, corresponding to the forward biasing of the diode. The sign change of transconductance, $\frac{dI_{DS}}{dV_{GS}}$, occurs at $V_{GS} = -5$ V, matching the hole current from WSe_2 with the electron current
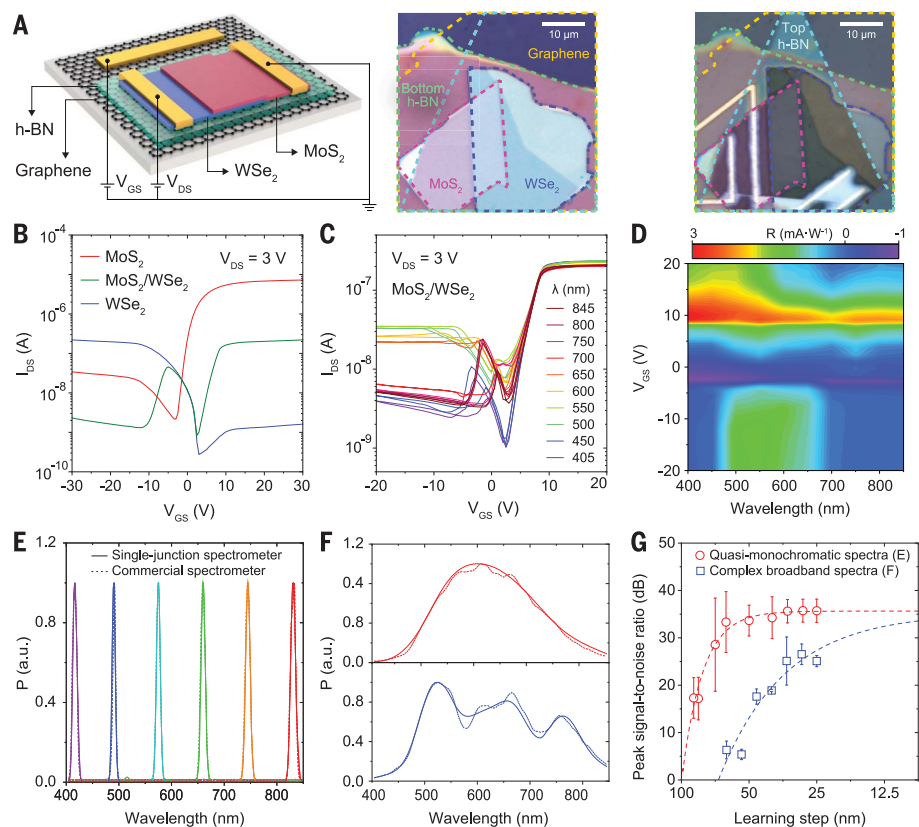

Fig. 2. Single-junction spectrometer demonstration. (A) Schematic of our MoS_2/WSe_2 heterojunction spectrometer (left) and its optical images on the h-BN and graphene layers before (middle) and after (right) depositing electrodes and stacking the top h-BN passivation layer. The top h-BN layer was omitted from the images in this panel for better visibility. **(B and C)** Transfer curves of the MoS_2 and WSe_2 channels and their heterojunction with the graphene gate without (B) and with (C) light illumination at different wavelengths with a fixed power of ~20 µW. **(D)** Color contour plot of the spectral response matrix. **(E and F)** Quasi-monochromatic [(E); bandwidth: ~10 nm] and two different broadband (F) spectra reconstructed with our spectrometer (solid curve) and measured using a commercial spectrometer (dashed curve). a.u., arbitrary units. **(G)** Peak signal-to-noise ratio between reconstructed and reference spectra as a function of learning step.

from MoS_2. This "anti-ambipolar" behavior and other transport properties (figs. S4 to S7) are typical of MoS_2/WSe_2 heterojunctions (22–28), providing clearly distinguishable V_{GS} dependence.

The transfer curves of the MoS_2/WSe_2 heterojunction measured under multiple known incident lights with a bandwidth of ~10 nm indicate a strong wavelength dependence (Fig. 2C). The photoresponsivity, $R = \frac{I_{ph}}{P}$, measured at different V_{GS} and incident light wavelengths is used to encode the spectral response matrix, where the photocurrent is defined as $I_{ph} = I_{light} - I_{dark}$, with I_{light} and I_{dark} representing I_{DS} with and without light illumination at $V_{DS} = 3$ V, respectively, and with P representing the incident light power (fig. S8). The gate-tunable spectral response of the MoS_2/WSe_2 heterojunction with high sensitivity over a wide spectral range is due to the wavelength-dependent absorption (29) of MoS_2 and WSe_2 as well as the controllable charge carrier transport (22–28) through the MoS_2/WSe_2 interface, unlike the

individual MoS_2 and WSe_2 materials. The spectral response matrix (Fig. 2D) inherits a rich structure from the dynamics of photoexcited charge carriers generated across the tunable MoS_2/WSe_2 heterojunction (22–29), confirming fast and stable spectral detection with giant gate tunability in our MoS_2/WSe_2 heterojunction (figs. S9 to S13).

After encoding this spectral response matrix (Fig. 2D) for the learning process, our single-junction spectrometer is ready to measure unknown incident light spectra, following the workflow diagram (fig. S2). Briefly, we measure the gate-tunable photocurrent of the unknown incident light and then compute its constrained least-squares solution to reconstruct the spectrum using an adaptive Tikhonov regularization method by minimizing the residual norm with a regularization factor (1, 8). Details of the optical setup, electrical and optoelectrical measurements, and computational reconstruction are provided in fig. S14 and materials and methods sections MM2 to MM4.
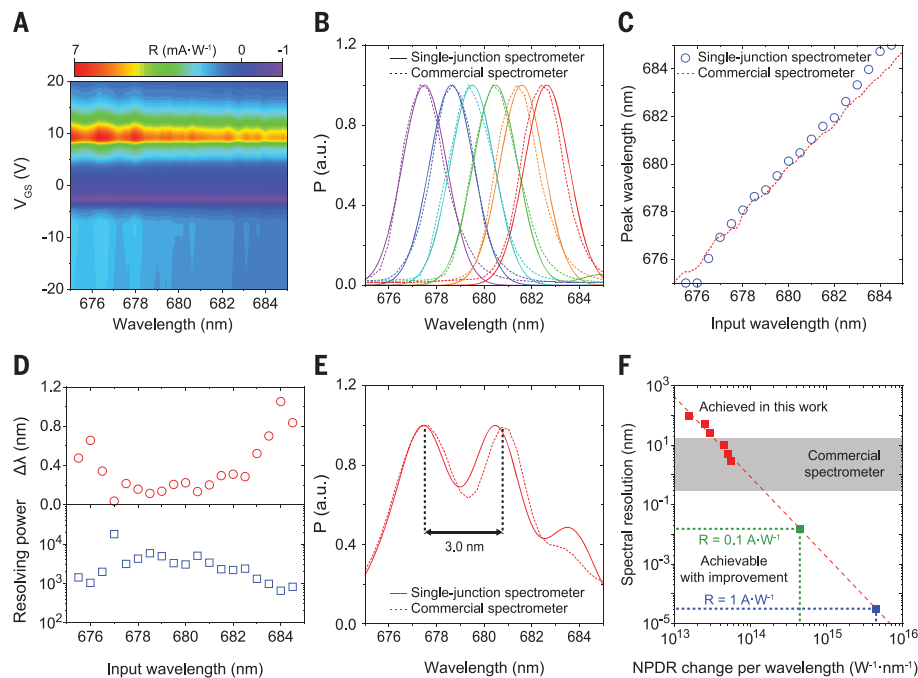
Fig. 3. High-performance wavelength resolving power and spectral resolution. (**A**) Color contour plot of the high-density spectral response matrix with a learning step of ~0.1 nm. (**B**) Monochromatic (bandwidth: ~2 nm) spectra reconstructed with our spectrometer (solid curve) and measured using a commercial spectrometer (dashed curve). (**C**) Peak wavelengths of the reconstructed and measured spectra as a function of input wavelength. (**D**) Peak wavelength difference between reconstructed and reference spectra (top) and wavelength resolving power of our single-junction spectrometer (bottom). (**E**) Complex spectra reconstructed (solid curve) and measured (dashed curve). (**F**) Future prospect of our single-junction spectrometer aiming for ultrahigh resolution.

The quasi-monochromatic and complex broadband spectra reconstructed with our single-junction spectrometer agree well with the reference spectra measured using a commercial spectrometer, demonstrating the viability of the single-junction spectrometer concept (Fig. 2, E and F). Although the demonstrated bandwidth (from ~405 to 845 nm) is limited because of the availability of the light wavelengths in our laboratory, the MoS_2/WSe_2 heterojunction exhibits photoresponse from ~400 to 2400 nm (*25*). Indeed, the vdW junctions are known to exhibit photodetection capability for incident light whose wavelength corresponds to about half of (or even much smaller than) the bandgap of each material (*15–17, 25*). Therefore, in principle, the single-junction spectrometer is not limited by the material bandgap and feasibly offers an operation bandwidth broader than that of our demonstration. Our single-junction spectrometer using the interlayer transport–mediated photoresponse is fundamentally different from the previously demonstrated spectrometer concepts, such as bandgap engineering and grading (*7–10*). Detailed comparisons of our work and the current state-of-the-art miniaturized spectrometers [including black phosphorus–based spectrometers with the Stark effect (*9*)] are given in supplementary text section ST2 and table S1.

To evaluate deviations between the reconstructed and reference spectra, the peak signal-to-noise ratio (PSNR) has previously been used to analyze the mean squared error (supplementary text section ST3). The maximum PSNR estimated from the extrapolation is ~35.7 and 33.6 dB for the quasi-monochromatic and complex broadband spectra, respectively (Fig. 2G). A reasonable learning step (i.e., a step in wavelength for encoding the spectral response matrix) can be chosen on the basis of the saturated PSNR. Therefore, a high-speed learning process is achievable with a large learning step and slightly reduced accuracy (*11*).

The wavelength-resolving power is an important measure of spectrometers in practical applications (*1, 2*). To demonstrate high spectral resolution capability with our single-junction ultraminiaturized spectrometer, we construct a high-density spectral response matrix through an ultrasmall learning step of ~0.1 nm using monochromatic light of wavelengths from ~675 to 685 nm for the learning process (Fig. 3A). Our single-junction spectrometer encoded by the high-density spectral response matrix can resolve monochromatic light with high accuracy (Fig. 3, B and C). The average peak wavelength difference ($\Delta\lambda$) between reconstructed and reference spectra is ~0.36 ± 0.06 nm, with a minimum of ~0.04 nm (Fig. 3D). This is comparable to the learning

step of ~0.1 nm. The average wavelength resolving power, $R_\lambda = \frac{\lambda}{\Delta\lambda}$ at a given input wavelength λ, is ~3470 (Fig. 3D).

Furthermore, we measure complex incident spectra to study the spectral resolution. Two peaks at ~679 nm, separated by ~3 nm, are successfully distinguished (Fig. 3E). Our spectrometer can also resolve broadband spectra and identify their peak wavelengths with high resolution (~0.9 nm, demonstrated in fig. S15). This indicates that our spectrometer has a spectral resolution comparable to or better than that of current state-of-the-art miniaturized spectrometers (*3–11*), with a footprint (~22 μm by 8 μm) comparable to or smaller than most. This footprint is several orders of magnitude smaller than that of commercial miniaturized spectrometers (*30*) and recently demonstrated spectrometers using metasurfaces (*4*), quantum dots (*6*), or a single-dot perovskite (*10*) (see table S1 for a detailed comparison). We note that the demonstrated accuracy (~0.36 nm) and resolution (~3 nm), which are limited by the smallest incident wavelength step available in our laboratory, can be further improved by minimizing the learning step during the learning process. We suggest that such a learning process—similar to the calibration process in traditional spectrometers—is practical for various applications.

Many strategies can be considered for improving the resolution, accuracy, and speed of our single-junction spectrometer (*1*). These include: (i) increasing the dataset size to create higher-density spectral response matrix by minimizing the learning step (*7–11*), (ii) designing junctions with higher response and larger wavelength or gate dependence (*15–17*), and (iii) optimizing the reconstruction algorithm [e.g., suppressing the perturbation with more advanced regularization (*1, 8*) or increasing the accuracy with convolutional processing (*20, 21*)]. Ideally, decreasing the learning step is a straightforward approach to forming a denser spectral response matrix for more accurate spectral reconstruction. However, there is a trade-off: Signal difference, measured at small learning steps, comparable to the measurement noise could result in errors during reconstruction.

To illustrate the future development possibilities of single-junction spectrometers, we consider the normalized photocurrent-to–dark current ratio (NPDR) change per wavelength step of two resolved peaks (supplementary text section ST4). The extrapolated line in Fig. 3F indicates the potential of our approach with improved photoresponsivity for higher resolution than the commercial miniaturized spectrometers (*30*). The achievable resolution is highlighted on the basis of recently reported photoresponse (~0.1 to 1 A·W⁻¹ at 532 nm) of MoS_2/WSe_2 heterojunctions (*25*). The resolution and bandwidth can be further improved by engineering junctions with different combinations of various
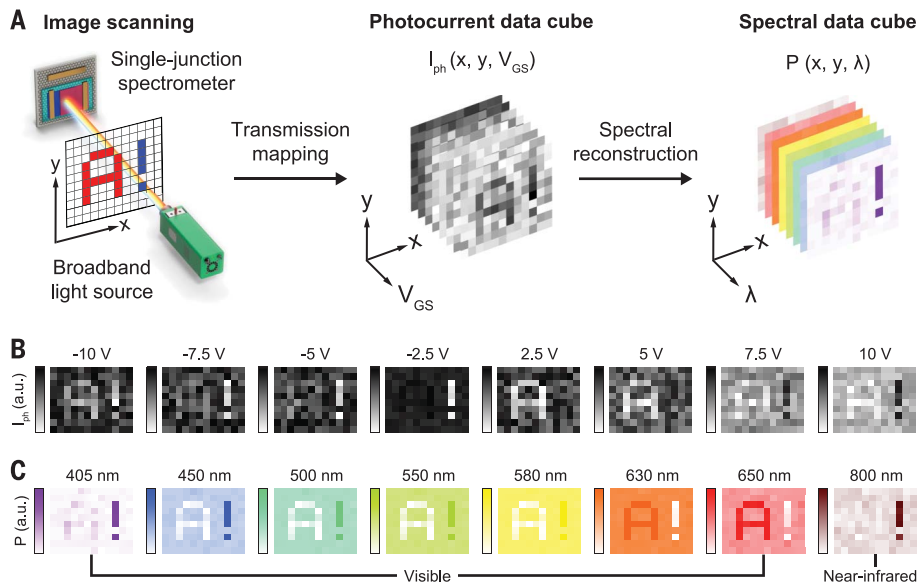
Fig. 4. Proof-of-concept demonstration of spectral imaging. (**A**) Configuration of spectral imaging using our single-junction spectrometer with a spatial scanning method. A broadband light source filtered with a color image is incident to our spectrometer for spectral imaging. (**B**) Photocurrent mapping data scanned at different V_{GS}. (**C**) Spectral images reconstructed at different wavelengths, covering the visible to near-infrared ranges. Higher intensity at each wavelength indicates that more broadband light is transmitted through the color image. The pixel intensity in (B) and (C) is normalized with each maximum intensity.

2D materials or integrating waveguides (*15–17*). Additional strategies for improving performance are provided in supplementary text section ST5. With the potential to substantially improve performance, our single-junction spectrometer can not only be adapted to other tunable junction architectures but also integrated with CMOS (complementary metal-oxide semiconductor)–compatible platforms.

Our single-junction spectrometer can benefit from the recently developed large-scale 2D material synthesis to construct an array for future spectral imaging. We demonstrate proof-of-concept spectral imaging of a color filter consisting of red, blue, and transparent areas with spatial scanning using our spectrometer (Fig. 4A). At each mapping position, the measured photocurrent data at different V_{GS} are recorded in the spatial response data cube for spectral reconstruction. A series of photocurrent mapping data scanned at different V_{GS} is displayed (Fig. 4B) and converted to a series of spectral data reconstructed at different wavelengths (Fig. 4C). The spectral images indicate that the red and blue filters absorb more incident broadband light from ~405 to 580 nm, and from ~600 to 700 nm, respectively. As a result, the spectra of the red uppercase letter "A" (from ~450 to 700 nm) and the blue exclamation mark "!" (from ~405 to 845 nm) are distinguishable from that of the background. Note that a strong light signal at near 800 nm for the exclamation mark can be fully detected, highlighting the advantages of spectral imaging over conventional RGB color im-

aging (see fig. S16 for the spectra reconstructed with different color filters). In our demonstration, the image resolution is defined by the mapping step. However, our concept has great potential for large-scale spectral imaging by future array devices, offering high spatial resolution with the junction at the micrometer or nanometer scale.

In our spectrometer, no photodetector array, filter array, or other bulky dispersive components are required to achieve high resolution, subnanometer accuracy, and broad operation bandwidth. The compact footprint of our single-junction spectrometers may provide scalability and compatibility with the current photonic integrated circuits and CMOS-compatible processes for direct integration into modern smartphones, lab-on-a-chip systems, and other customized devices ranging from bio-implants to drones and satellites.

Note added in proof: During the proofreading stage, we became aware of a recent work (*31*) using a $ReS_2/Au/WSe_2$ heterostructure, but with limited resolution and operation.

REFERENCES AND NOTES

1. Z. Yang, T. Albrow-Owen, W. Cai, T. Hasan, *Science* **371**, eabe0722 (2021).
2. R. F. Wolffenbuttel, *IEEE Trans. Instrum. Meas.* **53**, 197–202 (2004).
3. Z. Wang *et al.*, *Nat. Commun.* **10**, 1020 (2019).
4. A. Tittl *et al.*, *Science* **360**, 1105–1109 (2018).
5. D. M. Kita *et al.*, *Nat. Commun.* **9**, 4405 (2018).
6. J. Bao, M. G. Bawendi, *Nature* **523**, 67–70 (2015).
7. J. Meng, J. J. Cadusch, K. B. Crozier, *Nano Lett.* **20**, 320–328 (2020).
8. Z. Yang *et al.*, *Science* **365**, 1017–1020 (2019).
9. S. Yuan, D. Naveh, K. Watanabe, T. Taniguchi, F. Xia, *Nat. Photonics* **15**, 601–607 (2021).
10. L. Guo *et al.*, *Adv. Mater.* **34**, e2200221 (2022).
11. L. Kong *et al.*, *Nano Lett.* **21**, 9625–9632 (2021).
12. F. Xia, T. Mueller, Y. M. Lin, A. Valdes-Garcia, P. Avouris, *Nat. Nanotechnol.* **4**, 839–843 (2009).
13. M. Buscema *et al.*, *Chem. Soc. Rev.* **44**, 3691–3718 (2015).
14. F. H. Koppens *et al.*, *Nat. Nanotechnol.* **9**, 780–793 (2014).
15. A. K. Geim, I. V. Grigorieva, *Nature* **499**, 419–425 (2013).
16. M. M. Furchi, A. Pospischil, F. Libisch, J. Burgdörfer, T. Mueller, *Nano Lett.* **14**, 4785–4791 (2014).
17. N. Ubrig *et al.*, *Nat. Mater.* **19**, 299–304 (2020).
18. S. Wang *et al.*, *ACS Nano* **16**, 4528–4535 (2022).
19. Y. Sun, Y. Ding, D. Xie, *Adv. Funct. Mater.* **31**, 2105625 (2021).
20. S. Lee, R. Peng, C. Wu, M. Li, *Nat. Commun.* **13**, 1485 (2022).
21. L. Pi *et al.*, *Nat. Electron.* **5**, 248–254 (2022).
22. C.-H. Lee *et al.*, *Nat. Nanotechnol.* **9**, 676–681 (2014).
23. T. Roy *et al.*, *ACS Nano* **9**, 2071–2079 (2015).
24. A. Nourbakhsh, A. Zubair, M. S. Dresselhaus, T. Palacios, *Nano Lett.* **16**, 1359–1366 (2016).
25. M. Long *et al.*, *Nano Lett.* **16**, 2254–2259 (2016).
26. Y. Son *et al.*, *Nano Lett.* **16**, 3571–3577 (2016).
27. M.-H. Doan *et al.*, *ACS Nano* **11**, 3832–3840 (2017).
28. X. Sun *et al.*, *ACS Nano* **15**, 16314–16321 (2021).
29. H. S. Ra *et al.*, *Adv. Mater.* **34**, e2107468 (2022).
30. Hamamatsu, Mini-spectrometers product lineup; https://www.hamamatsu.com/eu/en/product/optical-sensors/spectrometers/mini-spectrometer.html.
31. W. Deng *et al.*, *Nat. Commun.* **13**, 4627 (2022).
32. H. H. Yoon, W. Cai, F. Nigmatulin, Spectral reconstruction based on tunable vdW junction spectrometers, version 1.1, Zenodo (2022); https://doi.org/10.5281/zenodo.7152385.

Science

Miniaturized spectrometers with a tunable van der Waals junction

Hoon Hahn YoonHenry A. FernandezFedor NigmatulinWeiwei CaiZongyin YangHanxiao CuiFaisal AhmedXiaoqi CuiMd Gius UddinEthan D. MinotHarri LipsanenKwanpyo KimPertti HakonenTawfique HasanZhipei Sun

Miniaturizing spectrometers

High-resolution spectrometry tends to be associated with bench-sized machines. Recent efforts on computational spectrometers have shown that this physical footprint can be shrunk by using nanowires and two-dimensional (2D) materials, but these devices are often associated with limited performance. Yoon *et al.* developed a single-detector computational spectrometer using an electrically tunable spectral response of a single junction comprising 2D van der Waal materials (see the Perspective by Quereda and Castellanos-Gomez). The electrically tunable spectral response and high performance of the tiny detector are promising for the further development of computational spectrometers. — ISO

View the article online
https://www.science.org/doi/10.1126/science.add8544
Permissions
https://www.science.org/help/reprints-and-permissions

Use of this article is subject to the Terms of service